MURA 85

MURA-LDF/1

INVESTIGATIONS OF f-IMPERFECTIONS IN AN ALTERNATING GRADIENT SYNCHROTRON WITH NON-LINEAR FORCES.

L. D. Fosdick
University of Illinois
and Midwestern Universities Research Association*
October 20, 1955

Errors in the machining and alignment of the focussing and defocussing 1/2-sectors in an alternating gradient synchrotron will perturb the motion of the accelerated particles and therefore place certain requirements on the size of the vacuum chamber. Since a large share of the cost of these machines depends on the size of the vacuum chamber, it is important to determine the requirements placed on it by such errors. Two common errors of this type are linear translations of the sectors and twists or rotations of the sectors. The former type are called f-imperfections and it is this class of imperfections which form the subject of the investigations reported on here.

The problem of f-imperfections in an alternating gradient machine with only linear forces present has been investigated by Courant(1) and Lüders(2). In these investigations it was assumed that the pair of equations governing the betatron oscillations were

---

* Assisted by the National Sciences Foundation

$$x'' + (1-n)x = 0$$
$$y'' + n\,y = 0 \qquad (1)$$

where the ' denotes differentiation with respect to the azimuthal coordinate, ϑ, and n is the field gradient. If one includes the non-linear cubic terms in these equations so that they become[3]

$$x'' + (1-n)x + \frac{e}{3}(x^3 - 3\,x\,y^2) = 0,$$
$$y'' + n\,y - \frac{e}{3}(3x^2y - y^3) = 0, \qquad (2)$$

then the difficulties encountered in treating f-imperfections are greatly increased.

The University of Illinois' High Speed Automatic Digital Computer, Illiac, and existing programs appeared to be a natural tool for investigating this problem. Accordingly, the necessary alterations were made in these programs and a study of the effect of f-imperfections in the presence of cubic forces was commenced.

At the time these investigations were begun two computer programs were available, one involved direct solution of the differential equations (2) by the Runge-Kutta method and the other iterated the transformations developed by J. Powell and R. Wright[4]. Since the latter program was considerably faster* and therefore more economical it was used in the initial studies.

---

*With the program using the transformations the computing time is about 3 seconds for 50 transformations (i.e., one circuit around a 50 sector machine) and with the differential equation this time becomes 100 seconds.

The Powell transformations are

$$\begin{aligned} T\,x &= a\,x + b\,x' + k\,b\,\left\{(1 + a)\,x + b\,x'\right\}^3 \\ T\,x' &= c\,x + a\,x' + k\,(1 + a)\left\{(1 + a)x + bx'\right\}^3 \end{aligned} \qquad (3)$$

where $a, b, c,$ are constants satisfying the condition $a^2 - bc = 1$ and k is an arbitrary constant; $a, b,$ and c are chosen to give the desired motion at small displacements and k is chosen by making a compromise between approximation to the form of the "invariant curves" of the correct solution and approximation to the betatron wavelength in the non-linear region. To simulate the f-imperfections these equations were altered as follows:

$$\begin{aligned} T(x - \Delta x_i) &= a(x - \Delta x_i) + bx' + kb\left\{(1+a)(x - \Delta x_i) + bx'\right\}^3 , \\ Tx' &= c(x - \Delta x_i) + ax' + k(1 + a)\left\{(1+a)(x - \Delta x_i) + bx'\right\}^3 , \end{aligned} \qquad (4)$$

where $i = (1, \ldots, N)$ and Δx_i is the magnitude of the i^{th} sector displacement.

It was recognized at the outset that the simulation of f-imperfections by this means was unrealistic. Since the transformation determines the coordinates of the particle at the center of the $i + 1$st focussing sector in terms of the coordinates of the particle at the center of the i^{th} focussing sector, Eqs. (4) describe the f-imperfections as if the "joints" occured only at the center of the focussing sectors, as illustrated in Fig. 1, rather than at every 1/2-sector as shown in Fig. 2.

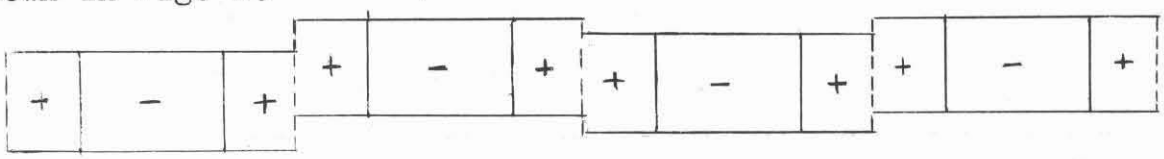

Fig. 1: Illustration of f-imperfections as simulated by use of Powell's transformation

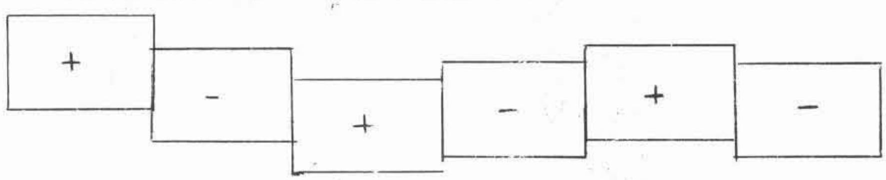

Fig. 2: Illustration of the usual picture of f-imperfections.

In spite of this difficulty it was felt that this procedure would be a useful starting point for the investigations and later, when transformations through focussing 1/2-sectors and defocussing 1/2-sectors became available they could replace Eqs. (4).

The machines investigated were assumed to have 50 sectors, each sector containing a focussing 1/2-sector and defocussing 1/2-sector. The constants used in the transformations for the investigations reported here correspond to $n = 253.303$, $e = 15{,}831.4$ and $\sigma = \pi/5.370$; this value for σ applies to the neighborhood of the origin of the phase plane. It follows from the scaling rules given by Powell[4] and the symmetry requirements imposed by 50 randomly displaced sectors that the field gradient, n, cannot be altered by scaling but the coefficient of the cubic term, e, can be scaled according to the following rule: If x and y are the variables in the unscaled system and X and Y are the variables in the scaled system, where

$$X = \frac{1}{s} x \ , \ Y = \frac{1}{s} y,$$

s = scaling constant

then the scaling of e is given by the relation

$$E = s^2 e.$$

The 50 random displacements for a particular machine were chosen from a Gaussian population. The abscissa of the Gaussian plot was quantized to allow for eighteen possible displacements, ranging from $(\pm)0.15$ to $(\pm)2.55$ in steps of 0.30; the displacements are given in units of the standard deviation. Colored chips were then made so that the number of chips of a given color was proportional to the probability of occurrence of a displacement of the corresponding magnitude. The chips were then placed in a box and drawn out at random, replacing each one ofter it was withdrawn, to obtain a set of fifty displacements. The sign of each displacement was determined by the flip of a coin. (Since this portion of the computation needs to be done only a small number of times, it was felt that it would be quicker to do it this way than to program the Illiac to do it.) The resulting list of 50 displacements was then used by the Illiac in the iteration of Eqs. (4). Ten such lists were made. With each set of 50 displacements the transformation program was run several times at different initial values of x, with the initial value of x' always zero. The value of x and x' after every 50 transformations was recorded by the Illiac. In addition, the maximum value of x obtained during each set of 50 transformations was also recorded; note that this applies only to the values of x obtained at the center of the focussing 1/2-sectors since this transformation is not capable of giving the value of x at any other point in the sector. With each set of initial values a total of 3,000 transformations was made. These computations give a family of apparently closed curves in the phase plane. In the neighborhood of the origin, where the effect of cubic terms is small, these curves are ellipses. Proceeding away from the origin the ellipses become distorted and finally at sufficiently large distances the points begin to scatter and do not appear to be on a smooth curve.* The coordinates of the equilibrium orbit at the observed azimuth of the perturbed machine are the coordinates of the center of the family of "closed" curves; they will be denoted by x(eq. orb.) and x'(eq. orb.) for x-motion and y(eq. orb.) and y'(eq. orb.) for y-motion; these quantities are tabulated in Tables 1, 2 and 3 on the following pages.

---

* It has often been suggested that scattering of the points, might indicate instability. However, N. Vogt-Nilsen has found in some cases that on careful examination "scattered" points do show regularities, indicating stability.

Computations were made for standard deviations of the displacement errors of 10^{-6}, 10^{-5}, 10^{-3}, 3×10^{-3} and 5×10^{-3}; these figures are given in units of the machine radius. If it is desired to scale the coefficient, e, of the cubic terms, then these numbers must be scaled according to the rules stated earlier. The two smaller values for the standard deviation 10^{-5} and 10^{-6}, are in the range of realistic values, thought to be achievable with careful engineering. The three large values must be scaled to bring them in the range of expected standard deviations.

In Table 1 are presented the coordinates of the equilibrium orbit in units of the standard deviation, ϵ, of the seqtor displacements for ten different sets of fifty sector displacements; all sets had the same standard deviation, equal to 10^{-6}.

Identification number of set of 50 displacements	$\frac{x \text{ (eq. orb.)}}{\epsilon}$	$\frac{x' \text{ (eq. orb.)}}{\epsilon}$	$\frac{y \text{ (eq. orb.)}}{\epsilon}$	$\frac{y' \text{ (eq. orb.)}}{\epsilon}$
1	5	< 20	5	< 20
2	5	20	5	20
3	< 5	20	< 5	20
4	< 5	< 20	< 5	< 20
5	< 5	< 20	< 5	< 20
6	< 5	< 20	< 5	< 20
7	< 5	20	< 5	20
8	< 5	< 20	< 5	< 20
9	< 5	< 20	< 5	< 20
10	< 5	20	< 5	20

Table 1 : Coordinates of the Equilibrium Orbit for 10 Sets of Sector Displacements with $\epsilon = 10^{-6}$, n = 253.303, e = 15,831.4.

The coordinates of the equilibrium orbit turned out to be so nearly zero that they are of the same order of magnitude as the round-off error for the computation. For this reason it is possible in some instances only to indicate that the coordinates are less than (<) some number, otherwise the figures in this table and in Tables 2 and 3 should be correct to about 20%.

In Table 2 are presented the results of another set of computations of the equilibrium orbit coordinates for ten sets of displacements. These computations differ from those making up Table 1 only in the fact that here $\epsilon = 10^{-5}$.

In Table 3 are presented the coordinates of the equilibrium orbit obtained from three sets of sector displacements, each with a different standard deviation, (much greater than the ones used in Tables 1 and 2).

Identification number of set of 50 displacements	$\frac{x \text{ (eq. orb.)}}{\epsilon}$	$\frac{x' \text{ (eq. orb.)}}{\epsilon}$	$\frac{y \text{ (eq. orb.)}}{\epsilon}$	$\frac{y' \text{ (eq. orb.)}}{\epsilon}$
11	3.0	2.0	3.0	2.0
12	3.5	8.0	3.5	8.0
13	0.5	12.0	0.5	12.0
14	0.5	2.0	0.5	2.0
15	0.5	2.0	0.5	2.0
16	0.5	6.0	0.5	6.0
17	2.0	12.0	2.0	12.0
18	0.5	2.0	0.5	2.0
19	2.0	4.0	2.0	4.0
20	1.5	12.0	1.5	12.0

Table 2 : Coordinates of the Equilibrium Orbit for 10 Sets of Sector Displacements with $\epsilon = 10^{-5}$, n = 253.303, e = 15,831.4.

Identification number of set of 50 displacements	$\frac{x \text{ (eq. orb.)}}{\epsilon}$	$\frac{x' \text{ (eq. orb.)}}{\epsilon}$	$\frac{y \text{ (eq. orb.)}}{\epsilon}$	$\frac{y' \text{ (eq. orb.)}}{\epsilon}$
21 (ϵ = 0.001)	2.74	0.52	2.79	0.68
22 (ϵ = 0.003)	2.55	0.07	3.11	1.45
23 (ϵ = 0.005)	2.20	1.08	5.51	14.9

Table 3: Coordinates of the Equilibrium Orbit for 3 Sets of Sector Displacements with Different ϵ and n = 227, e = 14.2×10^3.

For the runs made at standard deviations of 10^{-5} and 10^{-6} the character of the phase plots showed no qualitative differences for different sets of displacements for initial values of x in the range -.12 to - .12 with initial x' = 0 and for values of y in the range -.16 to -.16 with intial y' = 0 When the phase points were plotted to an accuracy of 5×10^{-4} (in units of the machine radius) the points obtained from runs with different sets of bumps with the same ϵ and the same starting values for x and x', all appeared to lie on the same smooth curve. The onset of scattering of the points occured at about the same point as found by Powell in runs made with no displacement errors. In the neighborhood of the equilibrium orbit the amount of cubic force was negligibly small, so in this region only linear effects were observed. The maximum value of the position coordinate, which was determined for each set of 50 transformations was always very nearly equal in magnitude to the initial position coordinate for the computation (initially, $x' = 0$, always); this was ture for all the computations discussed in this report.

For the runs made at $\epsilon = 0.001$, 0.003, and 0.005, the phase plots were quite noticeably affected. Scattering of the points on the phase plot occured in regions much closer to the origin than in the former runs with smaller displacements. Occasionally the presence of small "islands", where the points appeared to fall on a smooth, closed curve, could be detected. These islands lie outside the main family of closed curves, whose center defines the equilibrium orbit, and appear to be surrounded by a region in which the points scatter; the geometry is indicated in Fig. 3.

The dimensions of the region occupied by the main family of closed curves* is of obvious interest. Let us call the extent of this region in the x-dimension Δx stab., and its extent in the x'-dimension $\Delta x'$ stab., and similarly for the y-motion, Δy stab., $\Delta y'$ stab. It is to be noted that this measurement is somewhat subjective since scattering of the points on the phase plot is not a clearly defined thing.

---

*We sometimes refer to this as the stable region.

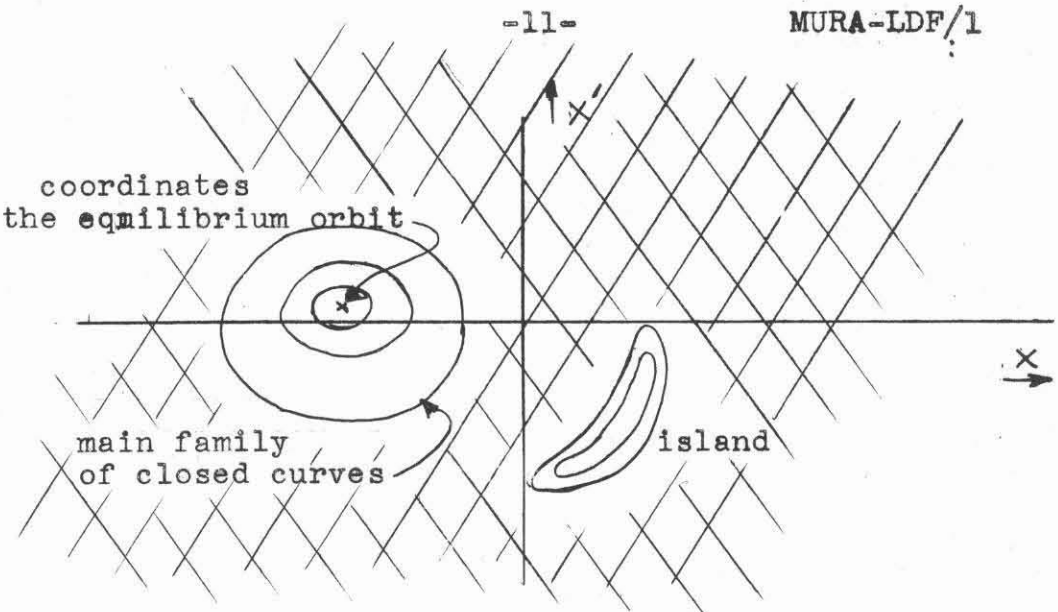

Fig. 3: A drawing to illustrate the appearance of islands. Scattering of the points appears in the region indicated by cross-hatching.

In Table 4 is listed our estimate of Δx stab, $\Delta x'$ stab, Δy stab and $\Delta y'$ stab for the different ϵ. These estimates have been made from the phase plots for the computations with different ϵ. It is clear from this table that the dimensions of the "stable region for the last three

ϵ	Δx_{stab}	$\Delta x'_{stab}$	Δy_{stab}	$\Delta y'_{stab}$
0	0.26	0.64	0.34	1.75
10^{-6}	0.24	0.64	0.32	1.75
10^{-5}	0.24	0.64	0.32	1.75
10^{-3}	0.12	0.40	0.2	0.88
3×10^{-3}	0.05	0.16	0.04	0.16
5×10^{-3}	0.02	0.08	0.02	0.08

Table 4 : Dimensions of the region in phase space occupied by the main family of closed curves, with n = 253,303, e = 15,831.4.

sets of displacements are considerably reduced. An interesting result is obtained by a computation of the ratio of the cubic force to the linear force, $\frac{ex^2}{3n}$, at the boundary of the stable region; for $\epsilon = 0$, 10^{-6}, 10^{-5} this ratio is about 0.3 for x-motion and about 0.55 for y-motion; for $\epsilon = 10^{-3}$, 3×10^{-3} and 5×10^{-3} it is 0.08, 0.03, and 0.01, respectively, for x- motion, and 0.21, 0.02, and 0.02, respectively, for y-motion. Thus for the large bumps scattering appears when the amount of cubic is quite small. It should be noted here that scaling does not effect the ratio $\frac{ex^2}{3n}$ so the result holds when the displacements are scaled down and e is correspondingly scaled up. This result was unexpected and at the present time is not clearly understood.

Finnally, some remarks should be made concerning the apparently small displacements of the equilibrium orbits presented in Tables 1, 2 and 3. Since we are dealing with a nearly linear system in the neighborhood of the equilibrium orbit we can compare these results with the theoretical results using the linear theory. Courant's equation gives a value for x eq orb.$/\epsilon$ of the order of 100 for the parameters we have used in the computation. Lüders' more accurate equation yields a value of approximately 25. Both of these figures are considerably greater than the ones we compute.

The source of this difficulty is clear. In the work of Courant and Lüders the physical picture of the imperfections is like that shown in Fig. 2 while we have really considered the situation shown in Fig. 1. If one tries to correct for this difference by dividing the results of Lüders by $\sqrt{2}$, (since we really consider 1/2 as many "bumps") the disagreement persists. Now in Fig. 1 it is noted that successive focussing and defocussing 1/2-sectors are, in effect, "tied together"... the displacement error between them being zero. It does not seem unreasonable to suspect that this situation can result in a smoothing of the perturbations caused by the bumps at the center of each focussing sector. This suspicion was confirmed when the following problem was investigated. Assume a purely linear machine and let successive pairs of focussing and defocussing 1/2 sectors be tied together, as shown in Fig. 4.

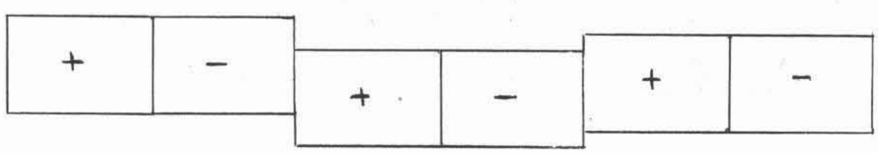

Fig. 4 : Illustration of the special case of f-imperfections treated in Appendix 1.

The assumption of linearity permits a relatively simple theoretical calculation of the displacement of the equilibrium orbit. This calculation is made in Appendix 1. In Appendix 2 we consider the physical situation illustrated by Fig. 2 in a linear machine and compute the displacement of the equilibrium orbit. The results of these two computations for a 50 sector machine with $n_+ = - n_-$, and equal length focussing and defocussing 1/2-sectors, are presented in Table 5.

	Appendix 1	Appendix 2
σ	$\frac{\sqrt{\overline{y^2}_{eq.orb.}}}{\epsilon}$	$\frac{\sqrt{\overline{y^2}_{eq.orb.}}}{\epsilon}$
$5\pi/6$	97	100
$\pi/2$	12	19
$\pi/3$	3.9	18
$\pi/4$	6.6	21
$\pi/6$	5.8	28
$\pi/20$	1.1	18

Table 5 : RMS displacement of the equilibrium orbit at the center of a focussing 1/2 sector in a 50 sector linear machine when +,- 1/2-sectors are "tied together" (col.1) and when they are not (col 2).

It is clear from this table that the RMS displacement of the equilibrium orbit is considerably smaller for the situation displayed in Fig. 3 than for that displayed in Fig. 2 when σ is in the range $\pi/3$ to $\pi/20$. This result supports the earlier conjecture that the small values obtained from the Illiac computation were due to successive focussing, defocussing 1/2-sectors having zero displacement with respect to each other.

tions is like that shown in Fig.2 while we have really considered the situation shown in Fig. 1. If one tries to correct for this difference by dividing the results of Lüders by $\sqrt{2}$, (since we really consider 1/2 as many "bumps") the disagreement persists. Now in Fig. 1 it is noted that successive focussing and defocussing 1/2-sectors are, in effect, "tied together"... the displacement error between them being zero. It does not seem unreasonable to suspect that this situation can result in a smoothing of the perturbations caused by the bumps at the center of each focussing sector. This suspicion was confirmed when the following problem was investigated. Assume a purely linear machine and let successive pairs of focussing and defocussing 1/2 sectors be tied together, as shown in Fig. 4.

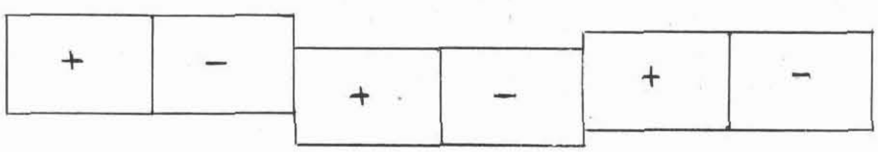

Fig. 4 : Illustration of the special case of f-imperfections treated in Appendix 1.

The assumption of linearity permits a relatively simple theoretical calculation of the displacement of the equilibrium orbit. This calculation is made in Appendix 1. In Appendix 2 we consider the physical situation illustrated by Fig. 2 in a linear machine and compute the displacement of the equilibrium orbit. The results of these two computations for a 50 sector machine with $n_+ = - n_-$, and equal length focussing and defocussing 1/2-sectors, are presented in Table 5.

	Appendix 1	Appendix 2
σ	$\frac{\sqrt{\overline{y^2_{eq.orb.}}}}{\epsilon}$	$\frac{\sqrt{\overline{y^2_{eq.orb.}}}}{\epsilon}$
$5\pi/6$	97	100
$\pi/2$	12	19
$\pi/3$	3.9	18
$\pi/4$	6.6	21
$\pi/6$	5.8	28
$\pi/20$	1.1	18

Table 5 : RMS displacement of the equilibrium orbit at the center of a focussing 1/2 sector in a 50 sector linear machine when +,- 1/2-sectors are "tied together" (col.1) and when they are not (col 2).

It is clear from this table that the RMS displacement of the equilibrium orbit is considerably smaller for the situation displayed in Fig. 3 than for that displayed in Fig. 2 when σ is in the range $\pi/3$ to $\pi/20$. This result supports the earlier conjecture that the small values obtained from the Illiac computation were due to successive focussing, defocussing 1/2-sectors having zero displacement with respect to each other.

The RMS displacement of the equilibrium orbit at $\sigma = \pi/6$ according to the computation of Appendix 1, is 5.8. This result is in agreement with those found from the Illiac computation. It is not surprising that such agreement is found since for the constants we have used the linear part of the Powell transformation (Eq. 4) corrsponds to a $\sigma = \pi/5.370$. This agreement of the results also indicates that the perturbations on the equilibrium orbit resulting from the imperfections illustrated in Fig. 4 do not differ significantly from those caused by the imperfections illustrated in Fig. 1.

Finally it should be remarked that one Illiac computation was made in which the Runge-Kutta method of solution of the differential equation was used rather than the Powell transformations. The imperfections were identical to those used with the Powell transformation equations (Fig. 1). The results of this computation were in good agreement with those obtained from the use of the transformations.

These results suggest an interesting idea. If, in the construction of an AG machine, it would be possible to construct each unit of the machine as a focussing-defocussing pair in such a way that the alignment error of the focussing 1/2-sector relative to the defocussing 1/2-sector within a unit was very small, then errors resulting from misalignment of the units themselves would cause much smaller perturbations of the equilibrium orbit than if the 1/2-sectors themselves were the units and laid down with the same misalignment errors. (We here ignore the obvious improvement of a factor of $\sqrt{2}$).

Appendix 1

In the following an equation for the RMS displacement of the equilibrium orbit at the center of a focussing sector in a conventional alternating- gradient synchrotron with linear forces and f-type imperfections like those shown in Fig. 4 of the text is derived.

In a perfect machine the betatron oscillations are described in phase space by the following matrix equation:

$$Y\,(\vartheta + \Delta\vartheta\,) = M\,(\vartheta + \Delta\vartheta\,|\,\vartheta\,)\quad Y\,(\vartheta), \tag{1}$$

where ϑ is the azimuth of the particle in the machine and $Y(\vartheta\,)$ is the two component vector describing the radial or

$$Y(\vartheta\,) = \begin{pmatrix} y\,(\vartheta) \\ y'(\vartheta) \end{pmatrix} \tag{2}$$

vertical position coordinate and its derivative, $y' = dy/d\vartheta$. The coordinate $y(\vartheta\,)$ defines the position relative to the equilibrium orbit. We assume that n, the field gradient, is a constant in focussing 1/2-sectors and defocussing 1/2-sectors. The matrix M in Eq. (1) is then defined by the following equations(6):

For $n = n_1 > 0$

$$M\,(\vartheta + \Delta\vartheta\,|\,\vartheta\,) = \begin{pmatrix} \cos\psi_1 & n_1^{-1/2}\sin\psi_1 \\ -n_1^{1/2}\sin\psi_1 & \cos\psi_1 \end{pmatrix} \tag{3}$$

where $\psi_1 = n_1^{1/2}\,\Delta\vartheta_1$.

For $n = -n_2 < 0$

$$M(\vartheta+\Delta\vartheta|\vartheta) = \begin{pmatrix} \cosh \Psi_2 & n_2^{-1/2} \sinh \Psi_2 \\ n_2^{1/2} \sinh \Psi_2 & \cosh \Psi_2 \end{pmatrix}, \quad (4)$$

where $\Psi_2 = n_2^{1/2} \Delta\vartheta_2$.

It is now assumed that the matrix equation, corresponding to Eq. (1), for the imperfect machine is

$$Y(\vartheta+\Delta\vartheta) - E_i = M(\vartheta+\Delta\vartheta \mid \vartheta) \left[Y(\vartheta) - E_i \right], \quad (5)$$

where the position coordinate $y(\vartheta)$ is still measured relative to the equilibrium orbit in the perfect machine, $M(\vartheta+\Delta\vartheta|\vartheta)$ is a transformation through a portion of the machine in which the magnet alignment error is constant, and E_i is a random vector describing the constant alignment error of the i^{th} portion of the machine. The random vector E_i is written

$$E_i = \begin{pmatrix} \epsilon_i \\ 0 \end{pmatrix} . \quad (6)$$

Thus ϵ_i describes the position error (a translation) of the i^{th} portion of the machine, and ϵ_i is defined to have the following statistical property:

$$\overline{\epsilon_i \ \epsilon_j} = \epsilon^2 \delta_{ij}, \qquad \delta_{ij} = \begin{Bmatrix} 0 & i \neq j \\ 1 & i = j \end{Bmatrix}, \quad (7)$$

where the bar denotes an average over an ensemble of machines with misalignments.

To treat the situation illustrated in Fig. 4 of the text we let each period of the machine have a misalignment given by E_i and $M = M(\vartheta_{i+1} | \vartheta_i)$ be the transformation through one period of the machine, from the beginning of one focussing sector to the beginning of the next focussing sector. Equation (5) now takes the form

$$Y_{i+1} - E_i = M (Y_i - E_i) , \tag{8}$$

or

$$Y_{i+1} = M Y_i + (1 - M) E_i . \tag{9}$$

Let there be N periods in the machine. It follows from Eq. (9) that (10)

$$Y_{1+N} = M^N Y_1 + M^{N-1} (1-M)E_1 + M^{N-2}(1-M)E_2+\ldots+(1-M)E_N$$

Now assume that the system is not on a resonance and require that $Y_{1+N} = Y_1$, then

$$Y_1 = (1-M^N)^{-1} (1-M)M^N \sum_{i=1}^{N} M^{-i} E_i , \tag{11}$$

gives the coordinates of the equilibrium orbit at the start of a focussing sector in the machine (in particular, the first focussing sector).

Let φ_1 and φ_2 be the eigenvectors of M with corresponding eigenvalues λ_1 and λ_2. Expanding E_i along φ_1 and φ_2 we have

$$E_i = a_i \varphi_1 + b_i \varphi_2 . \tag{12}$$

Substitution of Eq. (12) into Eq.(11) yields

$$Y_1 = \frac{1-\lambda_1}{1-\lambda_1^N}\lambda_1^N \sum_{i=1}^{N} a_i \lambda_1^{-i} \varphi_1 + \frac{1-\lambda_2}{1-\lambda_2^N}\lambda_2^N \sum_{i=1}^{N} b_i \lambda_2^{-i} \varphi_2 . \tag{13}$$

The displacement of the equilibrium orbit at the center of the 1st focussing sector is given by

$$\begin{aligned} Y(\vartheta_1 + \tfrac{\pi}{2N}) &= M(\vartheta_1 + \tfrac{\pi}{2N}|\vartheta_1)\, Y(\vartheta_1) + (1-M(\vartheta_1+\tfrac{\pi}{2N}|\vartheta_1))\, E_1 \\ &= \frac{1-\lambda_1}{1-\lambda_1^N}\lambda_1^N \sum_{i=1}^{N} a_i \lambda_1^{-i} \left[M(\vartheta_1 + \tfrac{\pi}{2N}|\vartheta_1)\,\varphi_1\right] \\ &+ \frac{1-\lambda_2}{1-\lambda_2^N}\lambda_2^N \sum_{i=1}^{N} b_i \lambda_2^{-i} \left[M(\vartheta_1 + \tfrac{\pi}{2N}|\vartheta_1)\,\varphi_2\right] \\ &+ (1-M(\vartheta_1 + \tfrac{\pi}{2N}|\vartheta_1))\, E_1 . \end{aligned} \tag{14}$$

From Eq. (3)

$$M(\vartheta_1 + \frac{\pi}{2N}|\vartheta_1) = \begin{pmatrix} \cos\psi_{1/2} & n_1^{-1/2}\sin\psi_{1/2} \\ -n_1^{1/2}\sin\psi_{1/2} & \cos\psi_{1/2} \end{pmatrix} \tag{15}$$

where

$$\psi_{1/2} = \frac{n_1^{1/2}\pi}{2N} . \tag{16}$$

Now the eigenvectors φ_1 and φ_2 are given by

$$\varphi_1 = \begin{pmatrix} 1 \\ \alpha \end{pmatrix} , \qquad \alpha = \frac{\lambda_1 - M_{11}}{M_{12}} , \tag{17}$$

$$\varphi_2 = \begin{pmatrix} 1 \\ \beta \end{pmatrix}, \qquad \beta = \frac{\lambda_2 - M_{11}}{M_{12}},$$

and the eigenvalues are

$$\lambda_1 = e^{i\sigma}, \qquad \lambda_2 = e^{-i\sigma}. \tag{18}$$

From Eq. (12)

$$\begin{aligned} \epsilon_i &= a_i + b_i, \\ 0 &= a_i\alpha + b_i\beta, \end{aligned} \tag{19}$$

so

$$a_i = \frac{\epsilon_i}{1-\frac{\alpha}{\beta}}, \qquad b_i = \frac{\epsilon_i}{1-\frac{\beta}{\alpha}}. \tag{20}$$

Note that $\varphi_1 = \varphi_2^*$, $\lambda_1 = \lambda_2^*$, $a_i = b_i^*$.

It follows from the above that the mean-square displacement of the equilibrium orbit, $\overline{y^2(\vartheta_1 + \frac{\pi}{2N})}$, is

$$\begin{aligned} \overline{y^2(\vartheta_1+\frac{\pi}{2N})} = {} & 2\,\frac{|1-\lambda_1|^2}{|1-\lambda_1^N|^2}\,|\lambda_1^N|^2\,\overline{\Big|\sum_{i=1}^{N} a_i\lambda_1^{-i}\Big|^2}\,\Big|\cos\psi_{1/2} \\ & + \alpha\, n_1^{-1/2}\sin\psi_{1/2}\Big|^2 \\ & + 2\mathrm{Re}\left\{\frac{(1-\lambda_1)^2}{(1-\lambda_1^N)^2}\,\lambda_1^{2N}\,\overline{\Big(\sum_{i=1}^{N} a_i\lambda_1^{-i}\Big)^2}(\cos\psi_{1/2}\right. \\ & \left. + \alpha\, n_1^{-1/2}\sin\psi_{1/2})^2\right\} + (1-\cos\psi_{1/2})^2\,\epsilon^2 \\ & + 2\mathrm{Re}\left\{\frac{1-\lambda_1}{1-\lambda_1^N}\,\lambda_1^{N-1}\,\overline{a_1\epsilon_1}(\cos\psi_{1/2} + \alpha n_1^{-1/2}\sin\psi_{1/2})\right\}, \end{aligned} \tag{21}$$

and the RMS displacement is given by $\sqrt{\overline{y^2(\vartheta_1 + \frac{\pi}{2N})}}$.
The last two terms on the right are small compared to the first two and if we neglect them, it is found after a little manipulation that

$$\overline{y^2(\vartheta_1 + \frac{\pi}{2N})} = \epsilon^2 N\left(\frac{1-\cos\sigma}{1-\cos N\sigma}\right) B - \epsilon^2 \tan\sigma/2 \;\cot N\sigma/2\, B$$
$$+ \epsilon^2 \tan\sigma/2 \cot N\sigma/2 \cos^2\psi_{1/2}, \tag{22}$$

where

$$B = \frac{1}{1-\cos 2\sigma} \Big(-M_{12}M_{21}\cos^2\psi_{1/2} + n_1^{-1/2}\left[\frac{M_{11}-M_{22}}{2}\right] M_{21}\sin\psi_1$$
$$+ n_1^{-1} M_{21}^2 \sin^2\psi_{1/2}\Big), \tag{23}$$

and the M_{ij}'s are the elements of the matrix $M = M(\vartheta_{i+1}|\vartheta_i)$, Eq. (8). The figures in the first column of Table 5 of the text were computed from Eq. (22).

Now consider a machine in which each 1/2-sector may be displaced an amount ϵ_i ($i = 1, 2\ldots 2N$). The equation describing the transformation of the phase vector in going through one period of the machine, from the start of one focussing sector to the start of the next focussing sector, is

$$Y_{i+2} = MY_i + M_D(1-M_f)E_i + (1 - M_D)\,E_{i+1}, \tag{24}$$

where M is defined as before, M_D is the matrix for the transformation through a defocussing 1/2-sector, M_f is the matrix for the transformation through a focussing 1/2-sector and E_i is the error vector with components ϵ_i and 0 as before.

Define

$$E_i' = M_D(1-M_f)E_i + (1-M_D)E_{i+1}, \tag{25}$$

then Eq. (24) becomes

$$Y_{i+2} = MY_i + E_i' \quad , \tag{26}$$

and it is easily seen that

$$\begin{aligned} Y_{1+2N} &= M^N Y_1 + M^{N-1}\,E_1' + M^{N-2}\,E_3' + \ldots + E_{2N-1}' \\ &= M^N Y_1 + M^N \sum_{i=1}^{N} M^{-i}\,E_{2i-1}' \quad . \end{aligned} \tag{27}$$

Following the same line as before it is assumed that the system is not on a resonance and it is required that $Y_{1+2N} = Y_1$, then

$$Y_1 = (1-M^N)^{-1}\,M^N \sum_{i=1}^{N} M^{-i}\,E_{2i-1}' \tag{28}$$

gives the coordinates of the equilibrium orbit at the start of a focussing sector in the machine.

Expand E'_{2i-1} along the eigenvectors of M, φ_1 and φ_2:

$$E'_{2i-1} = a'_{2i-1}\,\varphi_1 + b'_{2i-1}\,\varphi_2 \,. \tag{29}$$

Equation (28) can now be written

$$\begin{aligned} Y_1' &= \frac{\lambda_1^N}{1-\lambda_1^N} \sum_{i=1}^{N} \lambda_1^{-i}\, a'_{2i-1}\,\varphi_1 \\ &+ \frac{\lambda_2^N}{1-\lambda_2^N} \sum_{i=1}^{N} \lambda_2^{-i}\, b'_{2i-1}\,\varphi_2 \,, \end{aligned} \tag{30}$$

and the equation for the displacement of the equilibrium orbit, at the center of the 1st focussing sector is given by

$$\begin{aligned} Y\left(\vartheta_1 + \frac{\pi}{2N}\right) &= M\left(\vartheta_1+\frac{\pi}{2N}\Big|\vartheta_1\right) Y(\vartheta_1) + \left(1-M\left(\vartheta_1+\frac{\pi}{2N}\Big|\vartheta_1\right)\right)E_1 \\ &= \frac{\lambda_1^N}{1-\lambda_1^N} \sum_{i=1}^{N} \lambda_1^{-i}\, a'_{2i-1} \left[M\left(\vartheta_1+\frac{\pi}{2N}\Big|\vartheta_1\right)\varphi_1\right] \\ &+ \frac{\lambda_2^N}{1-\lambda_2^N} \sum_{i=1}^{N} \lambda_2^{-i}\, b'_{2i-1} \left[M\left(\vartheta_1+\frac{\pi}{2N}\Big|\vartheta_1\right)\varphi_2\right], \\ &+ \left(1-M\left(\vartheta_1+\frac{\pi}{2N}\Big|\vartheta_1\right)\right) E_1 \,, \end{aligned} \tag{31}$$

where the matrix $M(\vartheta_1 + \frac{\pi}{2N} | \vartheta_1)$ is defined by Eqs. (15) and (16) of Appendix 1.

The computation of the constants in the Eq. (29) is a little more tedious here. One finds

$$a'_{2i-1} = \left[(M_D)_{21} - M_{21} - \beta (M_D)_{11} + \beta M_{11}\right] \frac{\epsilon_{2i-1}}{\alpha - \beta} \tag{32}$$

$$+ \left[-(M_D)_{21} + \beta (M_D)_{11} - \beta\right] \frac{\epsilon_{2i}}{\alpha-\beta} \quad ,$$

where $(M_D)_{ij}$ is the i, j element of the matrix M_D, M_{ij} is the i, j element of the matrix M and α and β are given by Eq. (17) in Appendix 1.

Taking the y component of Eq. (31), squaring, and averaging yields

$$\overline{y^2(\vartheta_1 + \frac{\pi}{2N})} = \frac{N}{2\sin^2 N\frac{\sigma}{2}} \overline{|a'|^2} \quad \left| \cos\Psi_{1/2} + \alpha n_1^{-1/2} \sin \Psi_{1/2} \right|^2$$

$$- \frac{1}{2\sin^2 N\frac{\sigma}{2}} \left(\frac{\sin\sigma N}{\sin\sigma}\right) \mathrm{Re}\left\{ e^{-i\sigma} \overline{(a')^2} \left(\cos\Psi_{1/2} + \alpha n_1^{-1/2} \sin \Psi_{1/2}\right)^2 \right\} \tag{33}$$

$$+ \frac{1-\cos\Psi_{1/2}}{\sin N\frac{\sigma}{2}} \quad \mathrm{Re}\left\{ \overline{\epsilon_1 a'_1}\, i e^{i\sigma(N/2-1)} \left(\cos\Psi_{1/2} + \alpha n_1^{-1/2} \sin\Psi_{1/2}\right)\right\}$$

$$+ (1 - \cos\Psi_{1/2})^2 \; \overline{\epsilon^2} \; ,$$

and the RMS displacement is given by $\sqrt{\overline{y^2(\vartheta_1 + \frac{\pi}{2N})}}$.

The first two terms on the right of this equation are the dominating terms, and so long as $\sin\sigma N/\sin\sigma$ can be regarded as small compared to N only the first term is important. The figures in column 2 of Table 5 of the text were computed from Eq. (33) using only the first term on the right.

References

1) E.D. Courant: Azimuthal inhomogeneities in the a.g. synchrotron. I. Displacement of equilibrium orbits (February 25, 1953).

2) G.L. Luders : Orbit Instabilities in the New Type Synchrotron. CERN/T/GL-4 (March, 1953).

3) J.L. Powell : Non-Linearities in the A.G. Synchrotron. MAC-JLP-1

4) J.L. Powell and R.S. Wright: Non-Linearities in A.G. Synchrotrons. Part II. MURA-RW/JLP-5.

5) J.L. Powell: Non-Linearities in A.G. Synchrotron. MAC-JLP-3

6) M. Hammermesh: The Alternating-Gradient Synchrotron.